INT. J. NUM. HEAT FLUID FLOW, VOL. 2, 407–427 (1992)

ULTRA-SHARP SOLUTION OF THE SMITH–HUTTON PROBLEM

B. P. LEONARD

Center for Computational Mechanics, University of Akron, Akron, Ohio 44325-3903, USA

AND

SIMIN MOKHTARI

NASA Ames Research Center, Moffett Field, California 94035-1000, USA

ABSTRACT

In 1982, Smith and Hutton published comparative results of several different convection–diffusion schemes applied to a specially devised test problem involving near-discontinuities and strong streamline curvature. First-order methods showed significant artificial diffusion, whereas higher-order methods gave less smearing but had a tendency to overshoot and oscillate. Perhaps because unphysical oscillations are more obvious than unphysical smearing, the intervening period has seen a rise in popularity of low-order artificially diffusive schemes, especially in the numerical heat-transfer industry. This paper presents an alternative strategy of using non-artificially diffusive higher-order methods, while maintaining strictly monotonic transitions through the use of simple flux-limiter constraints. Limited third-order upwinding is usually found to be the most cost-effective basic convection scheme. Tighter resolution of discontinuities can be obtained at little additional cost by using automatic adaptive stencil expansion to higher order in local regions, as needed.

KEY WORDS Smith–Hutton problem Highly convective flow ULTRA-SHARP QUICK Non-oscillatory convection Sharp monotonic simulation Higher-order convection

INTRODUCTION

In a well-known paper published in 1982, Smith and Hutton presented results of several authors' attempts to numerically solve a specially devised test problem involving streamline curvature typical of recirculating flows and steep variations in the transported scalar[1]. Most schemes were able to handle the diffusion-dominated low-Péclet-number regime adequately; but in the important high-convection regime, Smith and Hutton concluded that convection modelling 'remains the art of compromise between diffusive and oscillatory errors.' In the intervening period, it seems that artificially diffusive low-order (blended first/second-order) convection–diffusion schemes, such as Patankar's 'power-law difference scheme' (PLDS)[2], have become more popular than higher-order potentially oscillatory methods such as the third-order QUICK scheme (Quadratic Upstream Interpolation for Convective Kinematics)[3]. Perhaps this is because the overshoot (or undershoot) problems associated with higher-order methods can lead to *obviously* unphysical results such as locally negative densities or turbulence kinetic energy, for example[4]. But the low-order methods' results are also usually highly unphysical—although perhaps not always obviously so.

It is not merely a matter of first-order-based methods being somewhat less accurate than higher-order techniques; a much more important point is that such methods are often not even

0961–5539/92/050407–21$2.00

Received November 1991

attempting to solve the original physical problem. Convection–diffusion schemes that revert to first-order upwinding for convection (while physical diffusion is ignored) under (even only moderately) high-convection conditions achieve (plausible looking) non-oscillatory results by replacing the high-convection physical problem with an (anisotropic) artificially diffuse *low*-convection numerical problem. Blended first/second-order schemes of this type, such as Patankar's PLDS (or the earlier first/second-order-switching 'Hybrid' method of Spalding[5]) have actually gained in popularity in recent years, especially in the numerical convective heat-transfer industry[6]. Both PLDS and Hybrid are inexpensive approximations to the so-called exponential difference schemes (EDS)[7], first described by Allen and Southwell[8] (and independently 'rediscovered' several times in the intervening period).

It should be stressed that EDS is designed to give the *exact* solution to a very specific convection–diffusion problem: steady, one-dimensional, source-free, constant-coefficient convection and diffusion of a scalar between specified upstream and downstream boundary conditions. Hybrid and (particularly) PLDS solve this problem quite accurately and inexpensively. But, as pointed out by Raithby[9] over fifteen years ago, if any of these (rather restrictive) conditions is relaxed, the use of EDS (or various approximations such as Hybrid or PLDS) may result in very serious unphysical consequences. Least troublesome is the generalization to variable coefficients and non-linearity (provided the other restrictions are maintained). EDS-based methods are best when used in steady quasi-one-dimensional situations (without strong source terms), such as unseparated boundary-layers[10] or flow in pipes or channels[11]. In such cases, the typical physical balance is between *grid-aligned* stream-wise convection (using first-order upwinding) and transverse physical diffusion (using second-order central differencing). Introduction of source terms can lead to significant error[3,12]. Unsteady one-dimensional simulations are notoriously artificially diffusive[13], and unsteady multidimensional results are pitifully inadequate[14]; for this reason, first-order methods are not usually used for transient calculations.

But by far the most serious misapplication of EDS-based methods is to steady flow oblique or skew to the grid. In such cases, as shown by deVahl Davis and Mallinson[15] more than fifteen years ago, anisotropic 'cross-wind' artificial numerical (or 'false') diffusion is introduced, proportional to the sine of twice the flow-to-grid angle, the grid mesh-size, and the absolute convecting velocity. Clearly, under high-convection conditions (typical of practical problems), the artificial cross-wind diffusion could be extremely large, unless the flow is virtually aligned with one of the grid coordinates. This has been verified in a number of simulations[9,16–19]. It should also be noted that EDS-based schemes either switch-off (Hybrid) or totally suppress (PLDS and EDS) physical diffusivity and viscosity under such conditions[19]. This means, in particular, that a typical engineering calculation using sophisticated and expensive multiple turbulence equations is, in fact, using the turbulence model *merely as a diagnostic to switch off its own contributions to* the governing conservation and turbulence equations! This perhaps explains why such methods are often rather insensitive to the particular form of the turbulence model being used[20].

The usual 'justification' for using Hybrid or PLDS for flows oblique or skew to the grid seems to be based on grid-refinement studies; i.e., the grid is refined to a point where the results do not seem to be changing very much[21]. But, for first-order methods, as shown later, the approach to true grid-independence is a notoriously slow process. For EDS-based methods, one cannot claim reasonable accuracy (or proper use of the turbulence model, for example) until the grid is refined to a point where the component grid Péclet (or Reynolds) numbers are everywhere $O(1)$ or less—in which case, Hybrid and PLDS are operating as classical second-order central differencing (so that the switching or blending strategy is not needed). The massive grid refinement (and concomitant expense) that this would call for under high-convection conditions is clearly impracticable. Because of relative algorithmic simplicity, low expense (*per grid-point* calculation), strong convergence properties, inherent monotonicity, and availability in well-known CFD codes such as TEACH[22] (and its descendants) and some commercial CFD

packages[23], Hybrid and PLDS remain very popular, especially in the numerical heat-transfer industry[24]. But, in the authors' opinion, in light of the above remarks, Hybrid or PLDS (or other first-order or exponential-based schemes) *should not be used* for practical calculations.

There is clearly a strong need for a conceptually simple (and computationally inexpensive) convection scheme giving highly accurate non-artificially diffusive and non-oscillatory results on practical grids under high-convection conditions; i.e., for grid Péclet (or Reynolds) numbers arbitrarily large. The same scheme should, of course, be able to handle the low-Péclet-number diffusion-dominated regime, as well. As will be shown in this paper, these apparently conflicting requirements are not incompatible. Third-order upwinding is the lowest-order convection scheme for which the leading truncation error is dissipative (involving even-order spatial derivatives) but not 'diffusive' (i.e., second-order derivatives)—by definition, leading truncation error in this case involves fourth-order spatial derivatives and, therefore, does not corrupt physical diffusion. As is well known, however, third-order upwinding in its basic form can give rise to unphysical overshoots or undershoots near regions involving rapid changes in the transported variable[3,4,18,19].

But, as shown later, it is a relatively simple matter to incorporate universal limiter constraints (applicable to any order of accuracy) giving tight monotonic resolution of near-discontinuities without corrupting the accuracy of the underlying scheme[18,19]. This universal limiter for tight resolution and accuracy implemented *via* a simple high-accuracy resolution program constitutes the ULTRA-SHARP strategy for high-convection modelling. The recommended method uses limited third-order upwinding (ULTRA-QUICK) as the basic convection–diffusion scheme; then, in local regions requiring even higher-order resolution, the algorithm automatically branches to a limited higher-order scheme (such as ULTRA-5th or ULTRA-7th upwind, described later) using adaptive stencil expansion, locally, controlled by a simple non-smoothness monitor. In terms of achieving a desired accuracy (compared with a known exact solution, for example), this strategy is optimal in terms of requiring the lowest overall computer cost. In other words, although low-order methods are less expensive *per grid point*, they require an exorbitantly fine grid (and, therefore, a very high total cost) to achieve a prescribed accuracy. By contrast, the higher cost (per grid point) of *very* high-order methods used *globally* is not completely offset by the lower cost of a concomitantly coarser grid. Somewhere in between these extremes, there is an optimal order giving best *computational efficiency*[25] (i.e., lowest total cost for a prescribed accuracy, or lowest error for a prescribed computational budget).

In the following sections the specifications of the Smith–Hutton test problem are briefly reviewed. Then, for reference, results are shown for a number of well-known convection–diffusion schemes; in particular: PLDS (representative of exponential-based schemes), second-order upwinding, and third-order upwinding (QUICK), using a conservative control-volume time-marching formulation in each case. Fifth- and seventh-order upwinding are also briefly discussed; as is typical of unlimited higher-order schemes, tighter resolution is offset by stronger oscillations. The concept of the universal limiter, based on normalized variables, is then briefly reviewed. Results are shown for limited third-order (ULTRA-QUICK) and an ULTRA-3rd/5th/7th-order scheme using local adaptive stencil expansion. Finally, a cost-effectiveness study shows the optimality of the third-order-based ULTRA-SHARP schemes.

THE SMITH–HUTTON TEST PROBLEM

The two-dimensional test problem devised by Smith and Hutton is concerned with steady-state convection and diffusion of a scalar field such as temperature, T, for example, in a particular prescribed velocity field, $\mathbf{v}(x, y)$, with a known constant diffusivity, D. The non-dimensional governing equation is:

$$\mathbf{v}\cdot\nabla T = \frac{1}{P\acute{e}}\nabla^2 T \tag{1}$$

introducing the (macroscopic) Péclet number:

$$Pé = \frac{V_{ref}L_{ref}}{D} = \text{const.} \tag{2}$$

using appropriate reference velocity and length scales. The flow domain considered is a rectangle: $-1 \leqslant x \leqslant 1$, $0 \leqslant y \leqslant 1$. And the velocity field is given by:

$$u = 2y(1 - x^2) \tag{3}$$

and

$$v = -2x(1 - y^2) \tag{4}$$

corresponding to a streamfunction:

$$\psi = -(1 - x^2)(1 - y^2) \tag{5}$$

Figure 1 shows the streamline pattern for this flow-field.

The inlet temperature profile is specified as

$$T_{in}(x) = 1 + \tanh[\alpha(1 + 2x)] \tag{6}$$

for $y = 0$ and $-1 \leqslant x \leqslant 0$, where α is a transition-steepness parameter (e.g., a large α-value implies a steep transition near $x = -0.5$). A typical profile is also shown in *Figure 1*. For $x = -1$, the left-hand boundary condition becomes:

$$T_b = T_{in}(-1) = 1 - \tanh \alpha \tag{7}$$

This is used as the boundary condition along the boundary streamline $\psi_b = 0$; i.e., at $x = \pm 1$ (for $0 \leqslant y \leqslant 1$) and at $y = 1$ (for $-1 \leqslant x \leqslant 1$). For α greater than about 3, this means that the boundary temperature is essentially zero, whereas the top of the inlet profile is very close to 2 as $x \to 0$. Smith and Hutton proposed $\alpha = 10$ as representative of a relatively sharp transition. In the present paper, two other values of α are used: $\alpha = 100$ (representative of a very sharp transition) and $\alpha = 5$ (representing a relatively smooth transition). Note that no physical

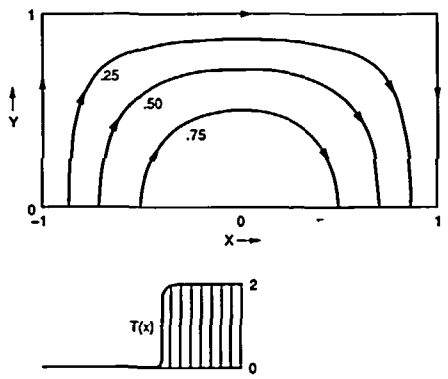

Figure 1 Streamline pattern and inlet temperature profile

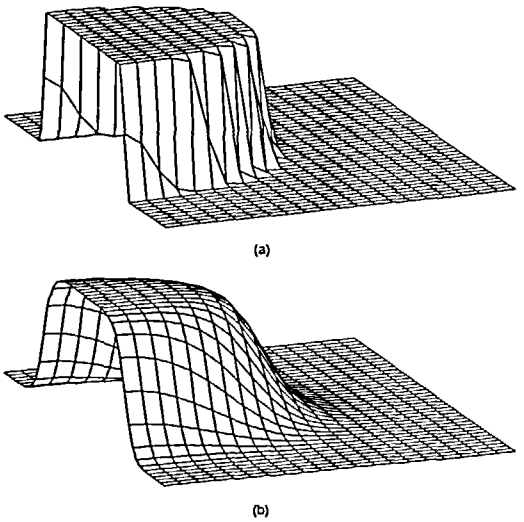

Figure 2 Three-dimensional portrayal of $T(x, y)$ for the infinite-$Pé$ solution. (a) $\alpha = 100$. (b) $\alpha = 5$

boundary conditions are specified at the outlet boundary, $y = 0$ $(0 \leqslant x \leqslant 1)$. Numerical boundary conditions equivalent to:

$$\left(\frac{\partial T}{\partial y}\right)_{y=0} = 0 \qquad \text{for} \quad 0 < x < 1 \tag{8}$$

are described below.

In the case of purely convective flow, $Pe = \infty$, the exact solution is easily obtained, since $T = \text{const.}$ along streamlines; i.e., $T = T(\psi)$. For example, at the inlet,

$$x = -\sqrt{1 + \psi}, \qquad -1 \leqslant x \leqslant 0 \tag{9}$$

so, throughout the flow domain when there is no diffusion,

$$T(\psi) = 1 + \tanh[\alpha(1 - 2\sqrt{1 + \psi})] = T(x, y) \tag{10}$$

using (5). In particular, this gives an outlet profile as the mirror-image of the inlet profile:

$$T_{\text{out}}(x) = 1 + \tanh[\alpha(1 - 2x)] \tag{11}$$

for $y = 0$ and $0 < x \leqslant 1$. *Figure 2* shows a three-dimensional portrayal of (10) on a 40 × 20 uniform mesh (41 × 21 grid-points, with $\Delta x = \Delta y$). In *Figure 2a*, $\alpha = 100$; whereas in *Figure 2b*, $\alpha = 5$.

Figure 3 shows portions of a typical staggered mesh used in the present analysis. Note that T-nodes are placed at boundaries. Boundary nodes shown as dots within squares correspond to specified boundary conditions; solid dots represent interior computed T-nodes; exterior pseudo-T-nodes (triangles) are also shown for use with higher order methods. Hollow circles represent ψ-nodes; these occur at the corners of temperature control-volume cells. This is shown in more detail in *Figure 4*. The staggered grid is a convenient arrangement, since *average* cell-face convecting velocities are then available by simple subtraction of stream-function values; e.g., referring to *Figure 4*, the average left-face convecting velocity is:

$$u_l = \frac{\psi_{TL} - \psi_{BL}}{\Delta y} \tag{12}$$

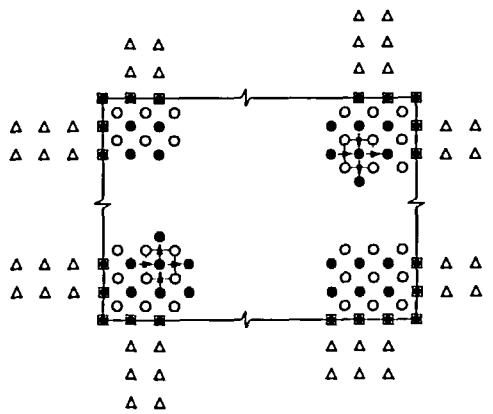

Figure 3 Schematic of staggered mesh. ○, Streamfunction nodes; ●, temperature nodes; Δ, external pseudonodes

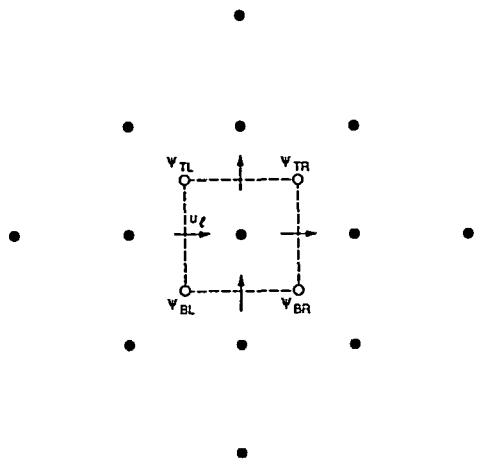

Figure 4 Detail of typical internal control-volume cell for the temperature transport equation

so that the corresponding average left-face normal Courant number component is:

$$\mathrm{CXL}(i,j) = \frac{(\psi_{TL} - \psi_{BL})\,\Delta t}{\Delta x\,\Delta y} \tag{13}$$

with an analogous formula for the bottom face.

Computation of interior node values of T follows a simple time-marching procedure. One first computes and stores the left and bottom face fluxes based on estimated face-values and normal gradients (peculiar to a given numerical interpolation scheme):

$$\mathrm{FLUXL}(i,j) = \mathrm{CXL}\cdot T_l - \frac{|\mathrm{CXL}|\,\Delta x}{\mathrm{PXL}}\left(\frac{\partial T}{\partial x}\right)_l \tag{14}$$

and

$$\mathrm{FLUXB}(i,j) = \mathrm{CYB}\cdot T_b - \frac{|\mathrm{CYB}|\,\Delta y}{\mathrm{PYB}}\left(\frac{\partial T}{\partial y}\right)_b \tag{15}$$

introducing local normal component cell face Péclet numbers:

$$\mathrm{PXL} = |u_l|\,P\acute{e}\,\Delta x \tag{16}$$

and

$$\mathrm{PYB} = |v_b|\,P\acute{e}\,\Delta y \tag{17}$$

The new values of T are then updated by a simple overwrite assignment statement,

$$\text{Set: } T(i,j) = T(i,j) + \mathrm{FLUXL}(i,j) - \mathrm{FLUXL}(i+1,j) + \mathrm{FLUXB}(i,j) - \mathrm{FLUXB}(i,j+1) \tag{18}$$

where flux conservation has been observed at each face. This is repeated until a converged steady state has been achieved, at which time all fluxes are in balance so that the update equation no longer changes the value of $T(i,j)$.

The treatment of the outflow numerical boundary condition is shown in *Figure 5*. Assume

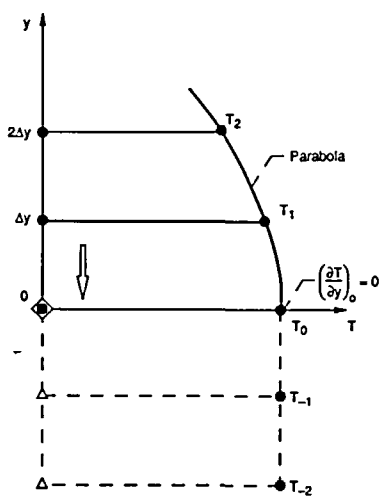

Figure 5 Outflow numerical boundary-condition treatment. Note that T_0 is determined by interpolating a parabola through T_2 and T_1 so that $(\partial T/\partial y)_0 = 0$

that $T(y)$ follows a parabola near the outlet for $y \geqslant 0$, with three conditions

$$T(2\Delta y) = T_2 \tag{19}$$

$$T(\Delta y) = T_1 \tag{20}$$

and

$$\left(\frac{\partial T}{\partial y}\right)_0 = 0 \tag{21}$$

Then, it is not hard to show that the corresponding value of T at the boundary is:

$$T_0 = \tfrac{4}{3}T_1 - \tfrac{1}{3}T_2 \tag{22}$$

The corresponding pseudonode values of T_{-1} and T_{-2} (used for fifth- and seventh-order upwinding) are taken to be simply:

$$T_{-1} = T_{-2} = T_0 \tag{23}$$

as shown in the Figure. Pseudonode values outside of the other boundaries are obtained by extrapolation (to an order consistent with the interior flux calculation) normal to the boundary, using the local physical boundary condition.

EXPONENTIAL-BASED SCHEMES

Exponential-based convection–diffusion schemes were first introduced into computational fluid dynamics by Allen and Southwell[8], and have been 'rediscovered' in various equivalent or approximate formulations by several people in the past thirty-seven years. Spalding's Hybrid scheme[5], Patankar's PLDS[2], and the algebraic approximation of Raithby and Schneider[7] can be interpreted as various levels of approximation to the exponential differencing scheme (EDS). It is fairly easy to show[19] that EDS is equivalent to using second-order central differencing for both convective and diffusive fluxes while replacing the actual grid Péclet (or Reynolds) number, P_Δ, with an effective value, P_Δ^*, that is itself a function of the physical P_Δ. The functional relationship is:

$$P_\Delta^* = 2\tanh(P_\Delta/2) \tag{24}$$

Spalding's Hybrid scheme can be interpreted as a very rough approximation to this, given by:

$$\left.\begin{aligned} P_\Delta^* &= P_\Delta \quad \text{for } 0 \leqslant P_\Delta \leqslant 2 \\ P_\Delta^* &\equiv 2 \quad \text{for } P_\Delta > 2 \end{aligned}\right\} \tag{25}$$

Patankar's power-law difference scheme represents a much more accurate approximation of the hyperbolic-tangent function:

$$\left.\begin{aligned} P_\Delta^* &= \frac{2P_\Delta}{P_\Delta + 2(1 - 0.1P_\Delta)^5} \quad \text{for } 0 \leqslant P_\Delta \leqslant 10 \\ P_\Delta^* &\equiv 2 \quad \text{for } P_\Delta > 10 \end{aligned}\right\} \tag{26}$$

The algebraic formulation of Raithby and Schneider can be interpreted as:

$$P_\Delta^* = \left[\frac{P_\Delta^2}{2(5 + P_\Delta^2)} + \frac{(1 + 0.005P_\Delta^2)}{P_\Delta(1 + 0.05P_\Delta^2)}\right]^{-1} \tag{27}$$

Note that here, too, $P_\Delta^* \to 2$ for large values of P_Δ. In fact, for EDS itself, (24), $P_\Delta^* \approx 2$ for $P_\Delta > 6$ (since $\tanh 3 = 0.995\ldots$). All three approximations are shown in *Figure 6* in relation to the hyperbolic-tangent curve.

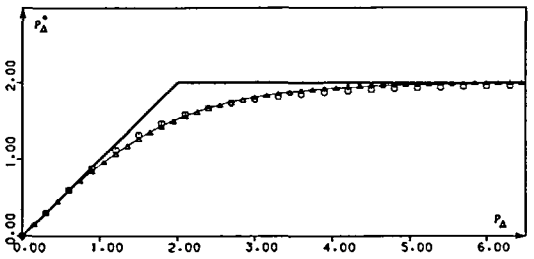

Figure 6 Comparison of Spalding's (piece-wise linear) Hybrid method, Patankar's power-law scheme (Δ), and Raithby and Schneider's algebraic approximation (○) with the exponential-differencing scheme (light continuous curve)

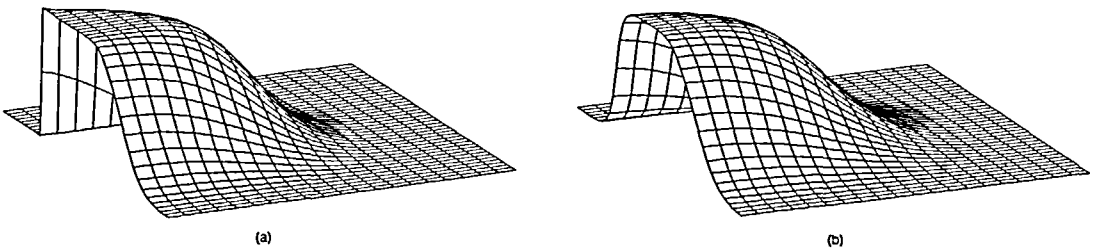

Figure 7 Infinite-*Pé* results for exponential-based schemes (equivalent to first-order upwinding) on a 40 × 20 mesh. (a) $\alpha = 100$, $\mathscr{E} = 0.135$; (b) $\alpha = 5$, $\mathscr{E} = 0.073$

For exponential-based schemes, the left-face flux, for example, is given by second-order central formulae for both face-value and normal gradient:

$$\mathrm{FLUXL}(i,j) = \frac{\mathrm{CXL}}{2}(T_{i,j} + T_{i-1,j}) - \frac{|\mathrm{CXL}|}{\mathrm{PXL}^*}(T_{i,j} - T_{i-1,j}) \tag{28}$$

where PXL* is the *effective* local x-component grid Péclet number at the left face, given by (24) or its approximation. Note that for PXL* = 2, the flux becomes

$$\mathrm{FLUXL}(i,j) = \mathrm{CXL} \cdot T_{i-1,j} \quad \text{for CXL} > 0 \tag{29}$$

or

$$\mathrm{FLUXL}(i,j) = \mathrm{CXL} \cdot T_{i,j} \quad \text{for CXL} < 0 \tag{30}$$

This, of course, corresponds to first-order upwinding for convection, with physical diffusion (computed but) ignored. This is what occurs in the Hybrid scheme for $P_\Delta > 2$, and in the other schemes (including EDS) for P_Δ greater than about 6, as seen in *Figure 6*.

Figure 7 shows 40 × 20 PLDS results for $Pé = \infty$; in this case the scheme is operating everywhere as first-order upwinding. The error reported in this and subsequent Figure captions is computed using

$$\mathscr{E} = \frac{1}{N}\sum |T_{\mathrm{comp}} - T_{\mathrm{ref}}| \tag{31}$$

where the summation is over all interior grid-points plus the outlet boundary, and N is the total number of grid-points involved, excluding pseudonodes (i.e., $N = 21 \times 11, 41 \times 21$, or 81×41).

By comparison with *Figure 2*, the PLDS simulation is seen to generate very artificially diffusive results. This is typical of exponential-based schemes. *Figure 8* gives inlet and outlet profiles using

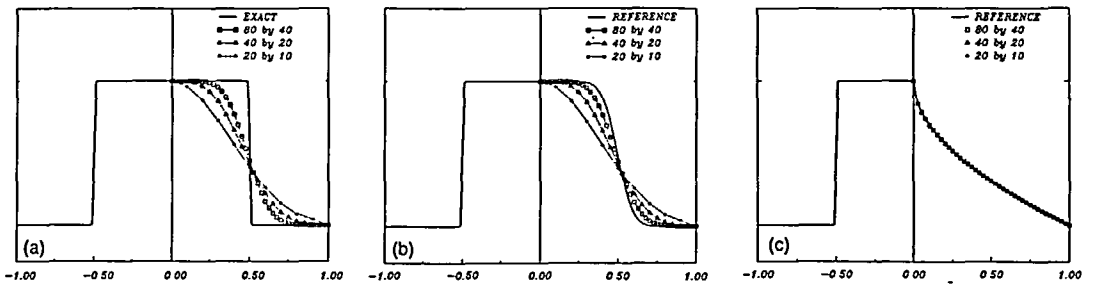

Figure 8 Inlet and outlet temperature profiles for $\alpha = 100$ using PLDS. (a) $Pé = \infty$; (b) $Pé = 500$; (c) $Pé = 10$

$\alpha = 100$ for $Pé = \infty$, 500, and 10, showing computed solutions on 20×10, 40×20, and 80×40 grids in each case, using PLDS. The reference finite-Péclet-number results have been obtained using the ULTRA-3/5/7 upwind scheme (described later) on a very fine (160×80) grid. For the larger-$Pé$ cases, the gross artificial diffusion of the exponential-based scheme is clear, indicating why such schemes should not be used for practical calculations. In the case of $Pé = 10$, local *grid* Péclet numbers are small and the scheme is equivalent to second-order central differencing. In this case, of course, there is no need for the blending (or switching, in the case of Hybrid) strategy to be used, as classical second-order central-differencing gives quite accurate and stable results, and can be made to converge very rapidly by using a deferred-correction technique[26,27].

SECOND-ORDER UPWINDING

When second-order upwinding is used for convection, it is conventional to use second-order central differencing for diffusion[25]. In this case, the left-face flux, for example, is given by:

$$\mathrm{FLUXL}(i,j) = \mathrm{CXL} \cdot T_l - \frac{|\mathrm{CXL}|}{\mathrm{PXL}}(T_{i,j} - T_{i-1,j}) \tag{32}$$

where the left-face convected value is:

$$T_l = \tfrac{3}{2}T_{i-1,j} - \tfrac{1}{2}T_{i-2,j} \quad \text{for CXL} > 0 \tag{33}$$

or

$$T_l = \tfrac{3}{2}T_{i,j} - \tfrac{1}{2}T_{i+1,j} \quad \text{for CXL} < 0 \tag{34}$$

Similar formulae are easily obtained for the bottom-face flux. Equations (33) and (34) can be combined into a single form valid for positive and negative convecting velocities by writing:

$$T_l = \tfrac{1}{2}(T_{i,j} + T_{i-1,j}) - \tfrac{1}{2}\,\mathrm{CURVNL} \tag{35}$$

defining the (upwind-weighted) 'normal curvature' at the left face as:

$$\mathrm{CURVNL} = \mathrm{CRVAVL} - \frac{\mathrm{SGN(CXL)}}{2}\mathrm{THIRDL} \tag{36}$$

where (suppressing the j-index, for convenience) the average (symmetric) second-difference across the left face is:

$$\mathrm{CRVAVL} = \tfrac{1}{2}(T_{i+1} - T_i - T_{i-1} + T_{i-2}) \tag{37}$$

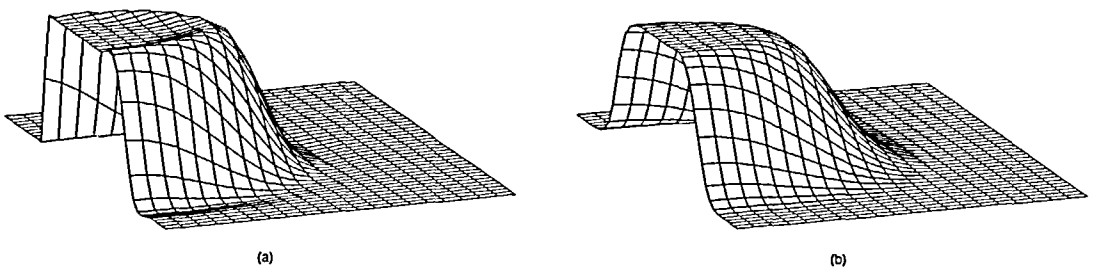

Figure 9 Infinite-*Pé* results for second-order upwinding on a 40 × 20 mesh. (a) $\alpha = 100, \mathscr{E} = 0.062$; (b) $\alpha = 5, \mathscr{E} = 0.014$

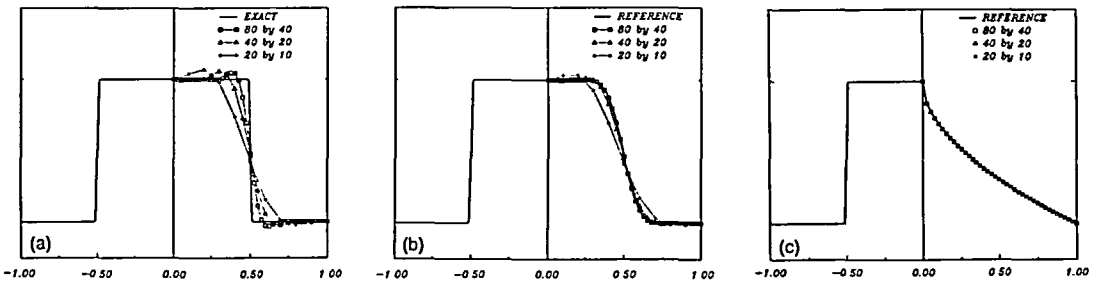

Figure 10 Inlet and outlet profiles for $\alpha = 100$ using second-order upwinding. (a) *Pé* = ∞; (b) *Pé* = 500; (c) *Pé* = 10

and the third-difference across the face is:

$$\text{THIRDL} = T_{i+1} - 3T_i + 3T_{i-1} - T_{i-2} \tag{38}$$

The infinite-*Pé* results for second-order upwinding are shown in *Figure 9*—as usual, for $\alpha = 100$ and 5. In this case, the smooth-inlet-transition results are quite good, with only a little numerical spreading and a very slight overshoot near the outlet; but note the significant overshoots and undershoots in the sharp-transition case. *Figure 10* shows grid-dependence results for *Pé* = ∞, 500, and 10, for $\alpha = 100$.

THIRD-ORDER UPWINDING (QUICK)

The two-dimensional QUICK scheme is the canonical third-order-upwind scheme for steady-state flow[4]. In this case, the left-face flux, for example, has the same form as (32); however, for consistency, the convected face-value includes both normal and *transverse* curvature effects, and the normal-curvature coefficient is much smaller than that shown in (35). Specifically, the QUICK left-face value is given by:

$$T_l = \tfrac{1}{2}(T_{i,j} + T_{i-1,j}) - \tfrac{1}{8}\,\text{CURVNL} + \tfrac{1}{24}\,\text{CURVTL} \tag{39}$$

where CURVNL is given by (36) and the upwind-weighted transverse-curvature term is:

$$\text{CURVTL} = T_{i-1,j+1} - 2T_{i-1,j} + T_{i-1,j-1} \quad \text{for CXL} > 0 \tag{40}$$

or

$$\text{CURVTL} = T_{i,j+1} - 2T_{i,j} + T_{i,j-1} \quad \text{for CXL} < 0 \tag{41}$$

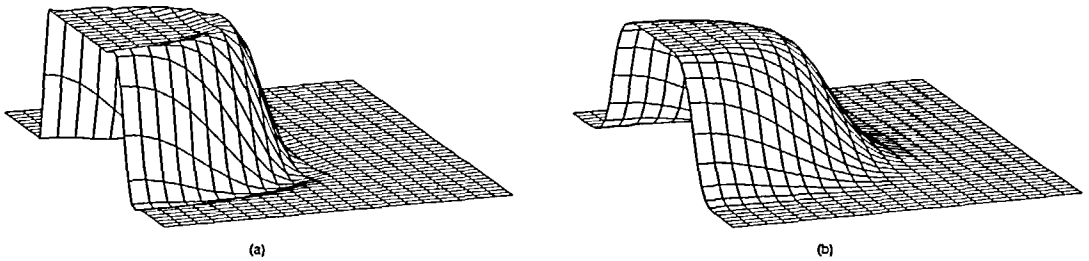

Figure 11 Infinite-*Pé* results using the QUICK scheme on a 40 × 20 mesh. (a) $\alpha = 100, \delta = 0.045$; (b) $\alpha = 5, \delta = 0.005$

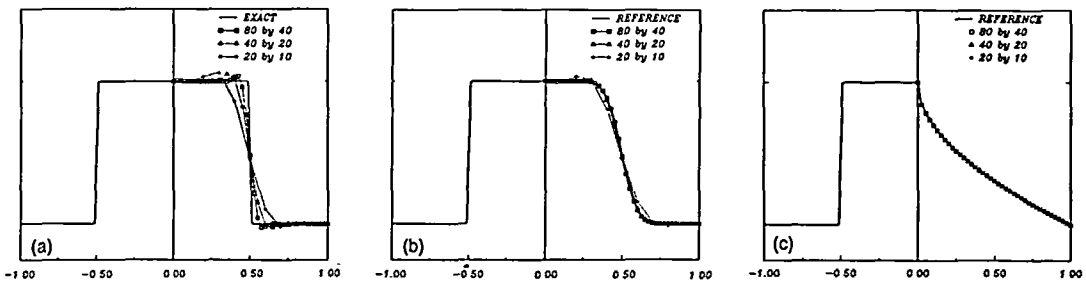

Figure 12 Inlet and outlet profiles for $\alpha = 100$ using the QUICK scheme. (a) $Pé = \infty$; (b) $Pé = 500$; (c) $Pé = 10$

Note that, consistent with bi-quadratic interpolation in the vicinity of the left face, the diffusive flux is identical to that obtained by central-differencing[4].

The QUICK results for $Pé = \infty$ are shown in *Figure 11*. The smooth-transition case is very well modelled; but, as with second-order upwinding, overshoots and undershoots occur in the sharp-transition simulation, although the computed transition itself is noticeably sharper in this case. Grid-dependence results are seen in *Figure 12*.

FIFTH- AND SEVENTH-ORDER UPWINDING

The fifth-order upwind algorithm used in this paper again takes the form of (32), but in this case, the recommended formula for the face-value is:

$$T_i = \tfrac{1}{2}(T_{i,j} + T_{i-1,j}) - \tfrac{1}{6}\,\mathrm{CRVAVL} + \tfrac{3}{128}\,\mathrm{FORTHL} + \tfrac{1}{24}\,\mathrm{CURVTL} \tag{42}$$

where (again suppressing j's for convenience) the upwind-weighted fourth difference is:

$$\mathrm{FORTHL} = T_{i+1} - 4T_i + 6T_{i-1} - 4T_{i-2} + T_{i-3} \quad \text{for CXL} > 0 \tag{43}$$

or

$$\mathrm{FORTHL} = T_{i+2} - 4T_{i+1} + 6T_i - 4T_{i-1} + T_{i-2} \quad \text{for CXL} < 0 \tag{44}$$

Three points should be mentioned:

(i) Higher-order terms are not used in the diffusive flux. This is appropriate because, when diffusion is large (small *Pé*), modelled profiles are smooth and the second-order form is entirely adequate; whereas, under high-convection conditions, the form of the small diffusion terms is not very important.

(ii) Higher-order transverse terms are not used in the convective flux. Although the third-order transverse curvature term is significant, numerical experimentation has shown that higher-order transverse terms have an almost negligible effect on results; but inclusion would add significantly to the cost of the calculation.

(iii) The coefficient of the normal-curvature term (1/6, rather than the theoretical value of 1/8) has been found to give slightly more accurate results in cases of scalar convection and diffusion, where exact solutions are available[19]. This was not found to be the case with third-order upwinding—where 1/8 seems to be optimal in all cases tested.

Figure 13 gives the fifth-order results for $Pé = \infty$. As perhaps expected, the large-α transition is sharper (than third-order) but generates significantly more overshoots, undershoots, and secondary ripples. The smooth transition is graphically indistinguishable from the exact result. Grid-dependence studies are again predictable and need not be shown here. Higher (for example, seventh) order upwinding merely accentuates the trends seen with fifth-order.

The seventh-order formula used in this study takes the form:

$$T_l = \tfrac{1}{2}(T_{i,j} + T_{i-1,j}) - \tfrac{1}{6}\,\mathrm{CRVAVL} + \tfrac{3}{128}\,\mathrm{FTHAVL} - \tfrac{1}{100}\,\mathrm{SIXTHL} + \tfrac{1}{24}\,\mathrm{CURVTL} \quad (45)$$

where (suppressing j's, as usual) the average (symmetric) fourth-difference across the left-face is:

$$\mathrm{FTHAVL} = \tfrac{1}{2}(T_{i+2} - 3T_{i+1} + 2T_i + 2T_{i-1} - 3T_{i-2} + T_{i-3}) \quad (46)$$

and SIXTHL is the upwind-weighted sixth-difference:

$$\mathrm{SIXTHL} = T_{i+2} - 6T_{i+1} + 15T_i - 20T_{i-1} + 15T_{i-2} - 6T_{i-3} + T_{i-4} \quad (47)$$

for CXL > 0. All indexes in SIXTHL are increased by 1 for CXL < 0.

UNIVERSAL LIMITER

The universal limiter is most easily described in terms of normalized variables. Let T_f represent the value of the convected scalar at any control-volume (CV) face; call the adjacent downstream

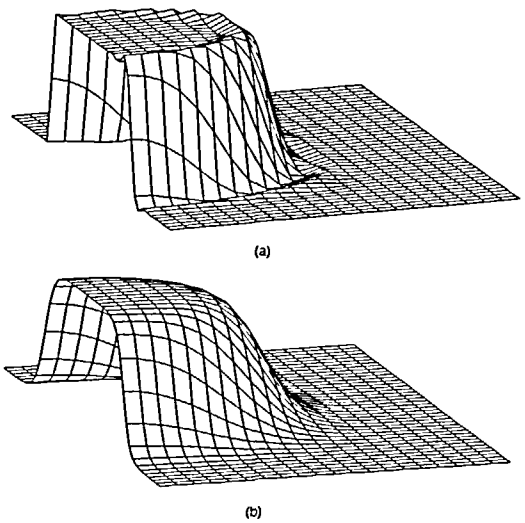

Figure 13 Infinite-*Pé* results using fifth-order upwinding on a 40 × 20 mesh. (a) $\alpha = 100$, $\delta = 0.036$; (b) $\alpha = 5$, $\delta = 0.003$

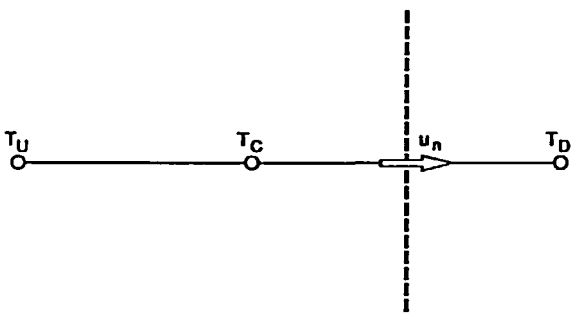

Figure 14 Definition of downwind (D), upwind (U) and central (C) nodes according to the direction of u_n at a control-volume face

node-value (in a direction normal to the face) T_D, the adjacent upstream node-value T_C, and the next upstream node-value T_U. *Figure 14* sketches the definition of these terms; as seen, node C lies between nodes U and D. Note, however, that the nodes involved are dependent on the sign of the normal convecting velocity component, u_n, at the CV face. Now define, anywhere in the vicinity of the face, a normalized variable:

$$\tilde{T}(x, y) = \frac{T(x, y) - T_U}{T_D - T_U} \tag{48}$$

In particular,

$$\tilde{T}_f = \frac{T_f - T_U}{T_D - T_U} \tag{49}$$

and

$$\tilde{T}_C = \frac{T_C - T_U}{T_D - T_U} \tag{50}$$

Note also that $\tilde{T}_U = 0$, whereas $\tilde{T}_D = 1$.

The universal limiter can be portrayed in the $(\tilde{T}_C, \tilde{T}_f)$ normalized-variable plane[18,19]. *Figure 15* shows the constraint boundaries. The basic idea behind the universal limiter is that, for $0 \leqslant \tilde{T}_C \leqslant 1$ (i.e., for locally monotonic node-values), $\tilde{T}_f$ should lie between upstream ($\tilde{T} = \tilde{T}_C$) and downstream ($\tilde{T} = 1$) normalized node-values (otherwise, interpolative monotonicity would be destroyed). It is also important that $\tilde{T}_f$ *not* lie in the second quadrant as this would allow oscillatory nodal behaviour[18]. The steep (but finite) slope, OB, is included to avoid indeterminacy near $\tilde{T}_C \to 0_+$. Some flexibility is allowed in the non-monotonic ranges ($\tilde{T}_C < 0$ or $\tilde{T}_C > 1$); the strategy shown ($\tilde{T}_f = \tilde{T}_C$) is one of the simplest possibilities. Note that first-order upwinding ($\tilde{T}_f \equiv \tilde{T}_C$ everywhere) marginally satisfies the limiter constraints. Clearly, this is the only 'linear' scheme (i.e., $\tilde{T}_f$ is a linear function of $\tilde{T}_C$) to give inherently monotonic results, as pointed out by Godunov[28] many years ago.

Use of the universal limiter proceeds as follows:

(i) First compute some (in general, high-order) estimate for the face value, T_f, and find the corresponding normalized values of $\tilde{T}_f$ and $\tilde{T}_C$.

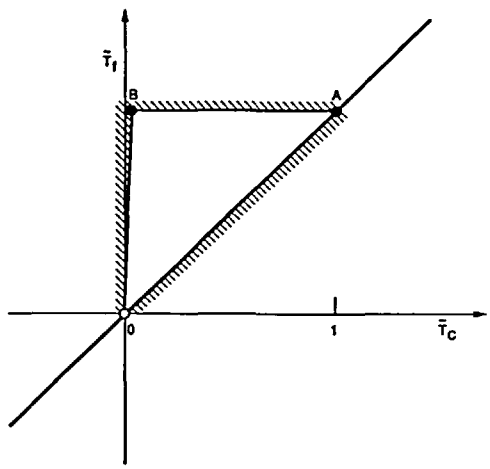

Figure 15 Portrayal of the universal-limiter constraints in the normalized-variable diagram

(ii) If the point $(\tilde{T}_C, \tilde{T}_f)$ satisfies the limiter constraints, proceed to step (iii); if not, reset $\tilde{T}_f$ to the nearest limiter-constraint at the same $\tilde{T}_C$ value.

(iii) Reconstruct the unnormalized face value:

$$T_f = \tilde{T}_f(T_D - T_U) + T_U \tag{51}$$

(iv) Use this value in combination with second-order diffusion in computing the total flux at the CV face; as, for example, in (32) for the left face.

ULTRA-QUICK results

When the universal limiter (for tight resolution and accuracy) is applied to the QUICK scheme (giving ULTRA-QUICK), overshoots and undershoots are automatically suppressed without additional smearing of the transition region. This is seen in *Figures 16* and *17*, which should be compared with *Figures 11* and *12*, and with *Figure 2*. Note the clean monotonic transition in the high-*Pé* large-α cases, as compared with the unlimited scheme. Smooth-region behaviour remains very good, reflecting the uniformly third-order accuracy of the basic algorithm.

Artificial compression

Figure 18 portrays a second-order convection scheme in the normalized-variable diagram, conforming to universal limiter constraints. The unconstrained portion of the scheme (DCB) consists of second-order central-differencing (DC) for $\tilde{T}_C \leqslant 0.5$

$$\tilde{T}_f = \tfrac{1}{2}(1 + \tilde{T}_C) \tag{52}$$

and second-order upwinding (CB) for $\tilde{T}_C \geqslant 0.5$

$$\tilde{T}_f = \tfrac{3}{2}\tilde{T}_C \tag{53}$$

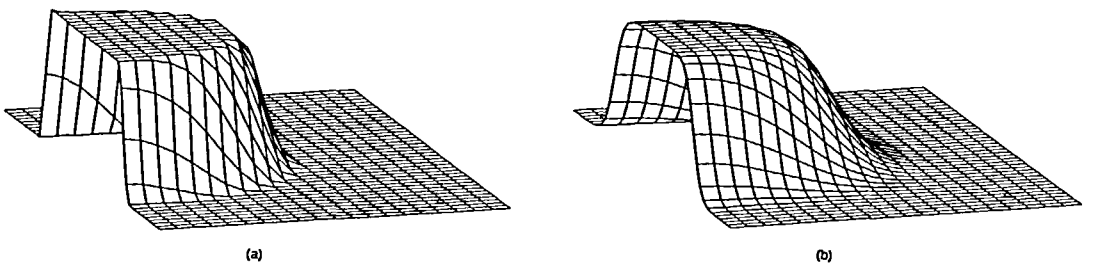

Figure 16 Infinite-*Pé* results using ULTRA-QUICK on a 40 × 20 mesh. (a) $\alpha = 100, \mathcal{E} = 0.034$; (b) $\alpha = 5, \mathcal{E} = 0.005$

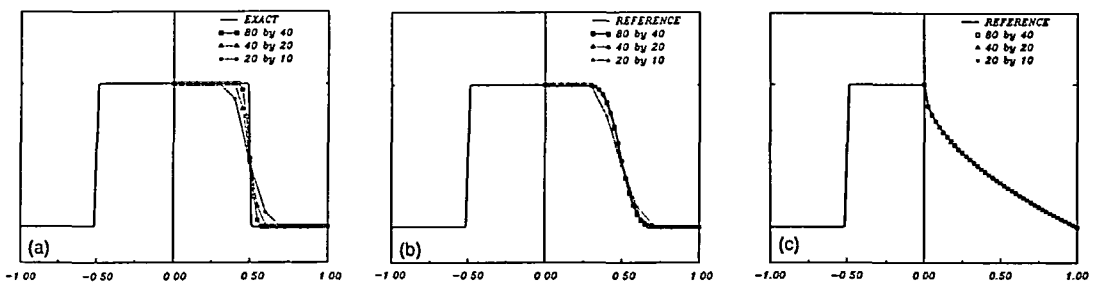

Figure 17 Inlet and outlet profiles for $\alpha = 100$ using the ULTRA-QUICK scheme. (a) $Pé = \infty$; (b) $Pé = 500$; (c) $Pé = 10$

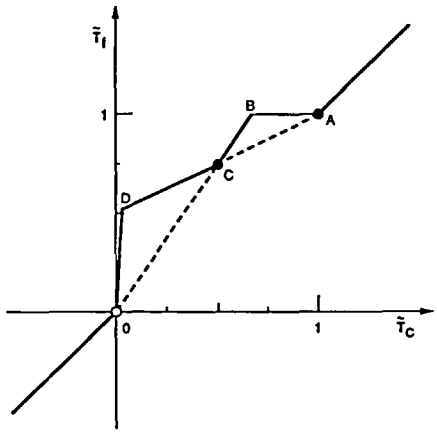

Figure 18 The Ultra-B scheme portrayed in the normalized-variable diagram

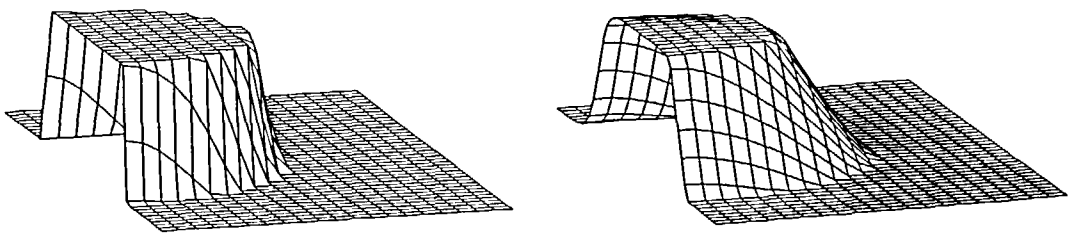

Figure 19 Infinite-*Pé* results using the Ultra-B scheme on a 40 × 20 mesh. (a) $\alpha = 100, \delta = 0.024$; (b) $\alpha = 5, \delta = 0.013$. Note the artificial steepening in case (b)

The upper constraint boundary (BA) can be interpreted as first-order *down*winding

$$\tilde{T}_f = 1 \tag{54}$$

This convection scheme has a tendency to introduce *negative* artificial diffusion into portions of simulated profiles. This can (artificially) enhance resolution of near-discontinuities—a phenomenon sometimes known as 'artificial compression'. The scheme was originally introduced by Roe[29] and named 'Ultra-B'; it is related to Roe's better-known 'Super-B' scheme, which is also artificially compressive[30]. In terms of simulating near-discontinuities, Ultra-B is indeed quite impressive for a second-order scheme. This is clearly seen in *Figure 19a* for the infinite-*Pé* sharp-transition case ($\alpha = 100$); but note the distortion of the initially smooth profile ($\alpha = 5$) in *Figure 19b*. As the profile is convected downstream, it becomes more and more ramp-like. This is due to the negative artificial diffusion inherent in artificially compression schemes. Similar artificial steepening effects occur with the finite-*Pé* simulations, as well. This is serious draw-back of artificial-compression methods[19]. The phenomenon can be avoided by using higher-order ULTRA-SHARP techniques, as described in the next section.

LOCAL ADAPTIVE STENCIL EXPANSION

Clearly, higher-order monotonic resolution of very sharp transitions could be obtained by using ULTRA-5th or ULTRA-7th globally. But in most of the flow domain, such high accuracy (and

concomitant cost) is not called for. It is of interest, from a cost-effectiveness viewpoint to construct an algorithm that would use ULTRA-QUICK in 'smooth' regions and automatically branch to a higher-order scheme *locally*, as needed. This strategy of local adaptive stencil expansion (as opposed to local adaptive grid refinement) is similar in many respects to the so-called '*p*-refinement' technique (as opposed to '*h*-refinement') used in some finite element methods[31]. The need for the local higher-order calculation—and correspondingly expanded stencil—can be determined by monitoring some suitable 'non-smoothness' parameter. One such quantity that comes to mind immediately is the local first-difference (proportional to the normal gradient) across a given CV face. For the left face, this would be:

$$\text{GRADL} = T_{i,j} - T_{i-1,j} \tag{55}$$

One also needs to detect local *changes* in gradient; the symmetrically placed average second-difference, defined in (37) for the left face, is suitable for this.

In smooth regions, both GRADL and CRVAVL will lie below certain pre-assigned thresholds; in this case, the basic ULTRA-QUICK algorithm is used. This will take care of the bulk of the flow domain since sharp transitions occur in narrow isolated regions, by definition. In fact, small curvature is equivalent to $\tilde{T}_C \to 0.5$, in which case the algorithm is automatically acting as an *unlimited* QUICK scheme. If CRVAVL exceeds the first threshold, THC1 ($= 0.1$ in the present study), the algorithm branches to ULTRA-5th *locally*; if it also exceeds THC2 ($= 0.7$), it branches further to ULTRA-7th. If GRADL exceeds THG ($= 0.35$), ULTRA-7th is used immediately. Clearly, other threshold strategies could be used; the procedure adopted here has evolved through computational experimentation over several test problems. It should be noted that the threshold constants are dimensional; i.e. a change in scale, for example, would require a corresponding change in threshold values. This problem can be avoided by rescaling the threshold constants with respect to an anticipated maximum absolute value of the convected variable occurring within the flow-field of interest (in the Smith–Hutton problem $|T|_{\max} = 2$).

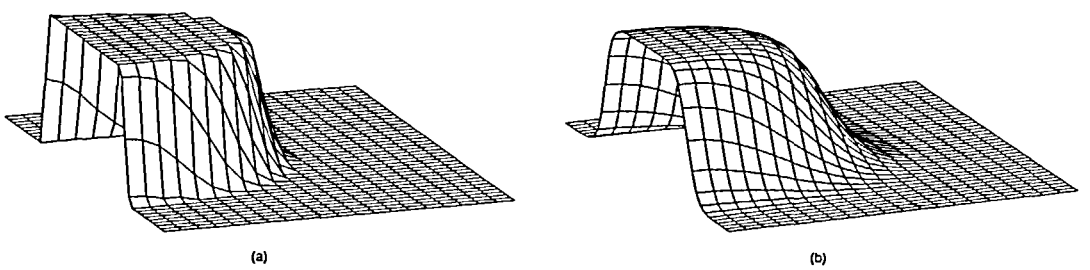

Figure 20 Infinite-*Pé* results using the ULTRA-3/5/7 adaptive-stencil-expansion method on a 40 × 20 mesh. (a) $\alpha = 100$, $\delta = 0.024$; (b) $\alpha = 5$, $\delta = 0.004$

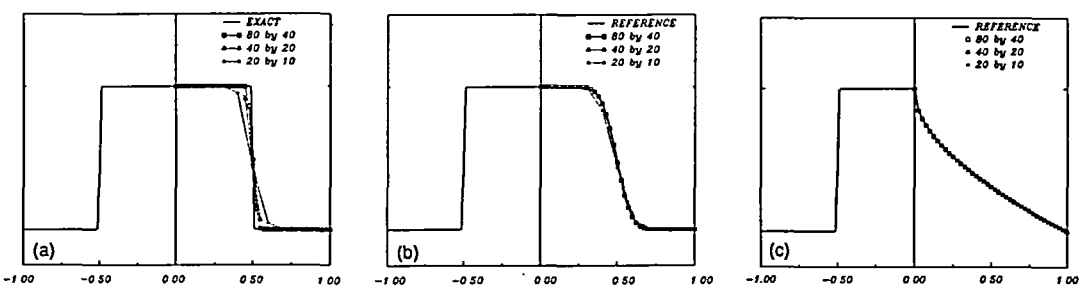

Figure 21 Inlet and outlet profiles for $\alpha = 0$ using ULTRA-3/5/7. (a) $Pé = \infty$; (b) $Pé = 500$; (c) $Pé = 10$

Figures 20 and *21* show results for the ULTRA-3rd/5th/7th scheme described above. Clearly, these are highly accurate results, even on the coarsest grid. As seen in the next section, the cost is only slightly more than the basic ULTRA-QUICK scheme but the *cost-effectiveness* (computational efficiency) is greatly enhanced.

OPTIMAL COST-EFFECTIVENESS

When dealing with higher-order convection schemes, one obvious question that comes to mind is: is it better (in terms of total cost) to use a low-order scheme on a very fine grid or a higher-order scheme on a coarser grid? Low-order schemes are relatively inexpensive per grid-point, but (as seen in the cases shown in this paper) require extremely fine grids for reasonable accuracy. On the other hand, the added expense (again, per grid-point) of very-high-order schemes may not be totally offset by a concomitant coarsening of the grid to achieve a given accuracy. To be more precise, assume that a desired level of accuracy has been pre-assigned for a problem that has a known exact solution, such as the infinite-*Pé* Smith–Hutton problem. Take any given convection scheme and solve on successively finer and finer grids until the desired level of accuracy has been achieved; simultaneously keep note of the CPU time (representing cost) at successive grid refinements. Repeat this process with other convection schemes. In this way, the cost for a prescribed global accuracy can be assigned to each scheme. Alternatively, one could specify an available computational budget and compute the corresponding accuracy of each scheme as the grid is refined.

Figure 22 gives the relevant information for the infinite-*Pé* Smith–Hutton problem with $\alpha = 100$. In part (a) of the Figure, the error, given by (31), is plotted *versus* N, on a log–log scale, for first-order upwinding, ULTRA-second-order upwinding (equivalent to the Chakravarthy–Osher scheme described by Sweby[32]), ULTRA-QUICK, ULTRA-5th, and ULTRA-7th upwind schemes, together with the ULTRA-3rd/5th/7th upwind scheme. Desired accuracy is shown by a broken line; for each scheme, the corresponding grid refinement can be found by interpolation. This is cross-plotted onto part (b) of the Figure which gives CPU-time as a function of N for each scheme. Part (c) of the Figure shows the error incurred by each method corresponding to a prescribed CPU-time in part (b). Alternatively, part (d) of the Figure gives the CPU-time for each method corresponding to the prescribed error in part (a).

From these results, one sees immediately that first-order upwinding (or a high-convection EDS-based scheme) is extremely inefficient because, although the cost-per-grid-point is low, the grid-refinement necessary for the desired accuracy would be extreme. Among the global higher-order methods, either ULTRA-QUICK or ULTRA-5th is seen to be optimal, depending on specific requirements of cost and accuracy; the 7th-order scheme is somewhat less efficient. The most cost-effective strategy of all, though, is to use local adaptive stencil expansion over the base third-order scheme. This is because the wider-stencil (more expensive) higher-order computation is automatically used very sparingly—only where needed: in isolated narrow regions involving a relatively few number of grid points. For flows involving only relatively smooth profiles (such as the $\alpha = 5$ infinite-*Pé* case), ULTRA-QUICK is again found to be optimal; in this case, the higher-order wider stencil is not called for. Similar conclusions have been reached with respect to other calculations on scalar and non-linear (Navier–Stokes) test-problems (such as the lid-driven cavity)[33].

CONCLUSION

The Smith–Hutton problem is an excellent test-problem for a numerical convection–diffusion scheme, especially in the high-convection regime. Strong streamline curvature and rapid local variation of the convected variable represent serious challenges to any numerical scheme. The

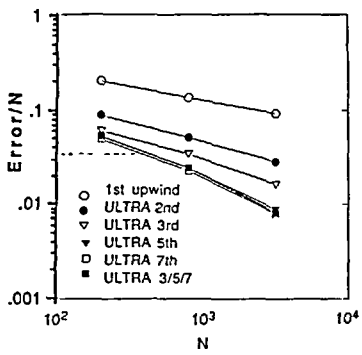

(a) Error *versus* grid refinement.

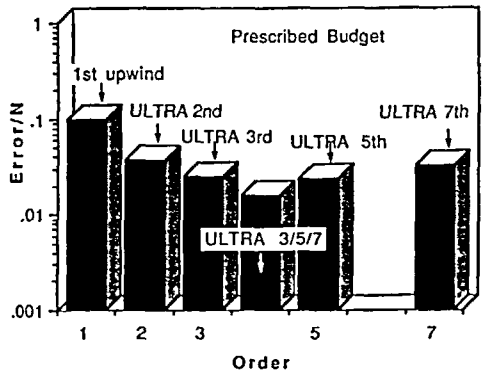

(c) Error for a prescribed budget.

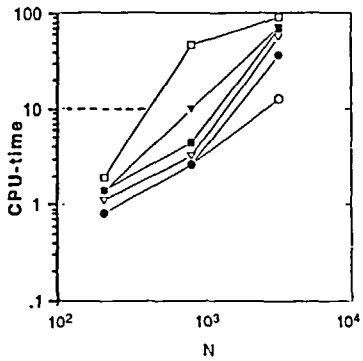

(b) Cost *versus* grid refinement.

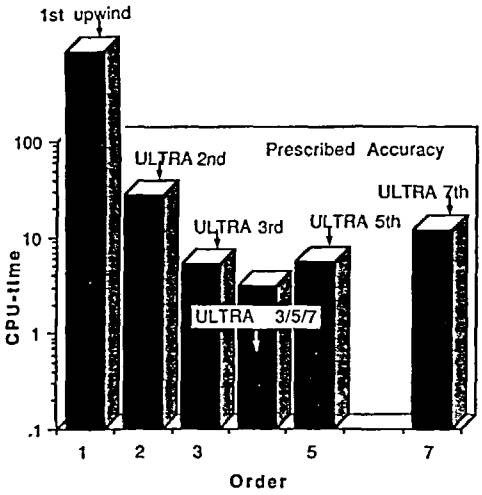

(d) Cost for a prescribed accuracy.

Figure 22 Computational efficiency of various non-oscillatory schemes for $\alpha = 100$ and $\dot{P}\acute{e} = \infty$. (a) Error *versus* grid refinement; (b) cost *versus* grid refinement; (c) error for a prescribed budget; (d) cost for a prescribed accuracy

availability of exact analytical solutions in the infinite-*Pé* case is very useful for a comparative error analysis. By choosing small values of α, the test-problem can be used for simulating smooth-function behaviour, as well. The present formulation of the problem uses a staggered grid, interleaving streamfunction and scalar nodes. Particular attention is paid to the outflow boundary condition, assuring $(\partial T/\partial y)_0 = 0$, consistent with local parabolic behaviour. The solution algorithm is based on explicit time-marching until a steady state is reached, although ADI tridiagonal solution of the steady equations can also be used[19,33].

Exponential-based schemes such as Spalding's Hybrid[5], Patankar's PLDS[2], or the algebraic approximation of Raithby and Schneider[7], all revert to first-order upwinding for convection with modelled physical diffusion (computed but) ignored or suppressed wherever the local normal component grid Péclet number exceeds 2 (Hybrid) or about 6 (for the other schemes,

including EDS itself). For most flows of practical interest, grid Péclet (Reynolds) numbers are likely to be far greater than 2 or 6 throughout most of the flow-field; under these conditions, exponential-based schemes are functioning as first-order upwinding almost everywhere, with physical diffusion switched off. The inherent artificial diffusion of such schemes is clearly evident, especially in the large-*Pé* cases. Slow grid-refinement convergence is also observed; this raises serious questions regarding grid-refinement claims made in support of exponential-based schemes. Such methods should be viewed as of historical interest only, and *should not be used* for serious practical applications.

Second-, third-, and higher-order upwind methods share a number of similar properties: as the order is increased, transition resolution becomes sharper, but overshoots and undershoots become more pronounced, with secondary ripples forming in the case of very-high-order schemes. Smooth function and low-*Pé* performance was seen to be generally very good, with error decreasing with order. The two-dimensional third-order (QUICK) scheme introduces transverse-curvature terms into the convective fluxes. Other calculations have shown that omission of these terms can incur significant error unless the grid is extremely fine[33]. As used in this study, higher-order schemes retain the third-order transverse curvature terms but omit higher-order transverse and other cross-difference terms; these are costly, algorithmically complex, and seem to have very little effect on the solution. It was also found unnecessary to extend diffusion modelling beyond second order.

The main draw-back of higher-order schemes is the generation of spurious unphysical overshoots and undershoots each side of sharp transition regions. This appears to be the main reason for a lack of interest in such methods as compared with essentially first-order schemes that produce monotonic, albeit extremely artificially diffusive, results. But it is a relatively straight-forward task to incorporate monotonizing flux-limiters into higher-order schemes, using the concept of a universal limiter. In terms of locally normalized variables, the universal limiter diagram is a simple triangular region with linear extensions on each side. When applied to higher-order convective fluxes, the universal limiter produces strictly monotonic results without introducing artificial diffusion and concomitant numerical spreading of (what should be sharp) transition regions. The tightness of the transition resolution increases as the order of the underlying scheme is increased. Using a higher-order ULTRA scheme was seen to be a better strategy than relying on artificial compression. The negative artificial diffusion inherent in second-order artificial-compression methods such as Ultra-B is responsible for extremely tight resolution of near-discontinuities; however, as was seen, it tends to distort smooth profiles into ramp-like transitions. In a recent paper, Tzanos[34] has also solved the Smith–Hutton problem using a third-order convection scheme with a simple limiting strategy essentially equivalent to ULTRA-QUICK (but without transverse curvature terms). Tzanos' paper also gives formulae for a variable (adaptive) grid. The results (for $\alpha = 10$ and $Pé = 1000$ or 10) are very similar to ULTRA-QUICK results for the same parameter values (slight differences are due to transverse-curvature terms and different treatment of numerical boundary conditions).

Among higher-order ULTRA schemes used globally, ULTRA-QUICK and ULTRA-5th were seen to be the best schemes in terms of cost-effectiveness: either lowest cost for a prescribed accuracy of lowest error for a prescribed cost, as the grid is refined. Local adaptive stencil expansion—using ULTRA-QUICK as the base scheme and automatically expanding the computational stencil to a higher-order ULTRA scheme locally (as needed)—was seen to be an extremely cost-effective technique, giving between fifth- and seventh-order accuracy for little more cost than that of the underlying third-order scheme. Optimal setting of the non-smoothness monitor thresholds requires some experimentation for each new problem; but it appears likely that a more general strategy will evolve as experience is gained with this new technique.

The ULTRA-SHARP strategy is ideally suited to steady-state Navier–Stokes calculations, as well[33]. If a turbulence model is used, the physics of the model is faithfully represented. Very narrow shear-layers oblique or skew to the grid can be accurately simulated without fear of artificial smearing or oscillation. It is a straightforward exercise to extend the conservative

finite-volume flux-based algorithms to three dimensions; and because of the high accuracy obtainable on very coarse grids, reliable three-dimensional simulations should soon become practicable for routine engineering calculations.

ACKNOWLEDGEMENTS

Portions of this work were supported by the National Science Foundation under contract ECS-8904595. The first author's research was also partially supported by the Institute for Computational Mechanics in Propulsion (ICOMP) at the NASA Lewis Research Center under Space Act Agreement C-99066-G.

REFERENCES

1 Smith, R. M. and Hutton, A. G. The numerical treatment of advection: A performance comparison of current methods, *Num. Heat Trans.*, **5**, 439–461 (1982)
2 Patankar, S. V. *Numerical Heat Transfer and Fluid Flow*, Hemisphere, New York (1980).
3 Leonard, B. P. A stable and accurate convective modeling procedure based on quadratic upstream interpolation, *Comp. Meth. Appl. Mech. Eng.*, **19**, 59–98 (1979)
4 Leonard, B. P. Elliptic systems: Finite difference method IV, *Handbook of Numerical Heat Transfer* (Eds. W. J. Minkowycz *et al.*), Wiley, New York, pp. 347–378 (1988)
5 Spalding. D. B. A novel finite difference formulation for differential expressions involving both first and second derivatives, *Int. J. Num. Meth. Eng.*, **4**, 551–559 (1972)
6 Lewis, R. W. and Morgan, K. (Eds.), *Numerical Methods in Thermal Problems*, Vol. VI, Pineridge Press, Swansea (1989)
7 Raithby, G. D. and Schneider, G. E. Elliptic systems: Finite-difference method II, *Handbook of Numerical Heat Transfer* (Eds. W. J. Minjowycz *et al.*), Wiley, New York, pp. 241–294 (1988)
8 Allen, D. N. de G. and Southwell, R. V. Relaxation methods applied to determine the motion, in two dimensions, of a viscous fluid past a fixed cylinder, *Q. J. Mech. Appl. Math.*, **8**, 129–145 (1955)
9 Raithby, G. D. A critical evaluation of upstream differencing applied to problems involving fluid flow, *Comp. Meth. Appl. Mech. Eng.*, **9**, 75–103 (1976)
10 Reddy, D. R. and Rubin, S. G. Consistent boundary conditions for reduced Navier–Stokes (RNS) scheme applied to three-dimensional viscous flows, *J. Fluids Eng.*, **110**, 306–324 (1988)
11 Hirai, S., Takagi, T. and Matsumoto, M. Predictions of the laminarization phenomena in an axially rotating pipe flow, *J. Fluid Eng.*, **110**, 424–430 (1988)
12 Leonard, B. P. A consistency check for estimating truncation error due to upstream differencing, *Appl. Math. Modelling*, **2**, 239–244 (1978)
13 Leonard, B. P. The ULTIMATE conservative difference scheme applied to unsteady one-dimensional advection, *Comp. Meth. Appl. Mech. Eng.*, **88**, 17–74 (1991)
14 Munz, K.-D. On the numerical dissipation of high resolution schemes for hyperbolic conservation laws, *J. Comp. Phys.*, **77**, 18–39 (1988)
15 de Vahl Davis, G. and Mallinson, G. D. An evaluation of upwind and central difference approximations by a study of recirculating flow, *Comp. Fluids*, **4**, 29–43 (1976)
16 Leschziner, M. A. Practical evaluation of three finite difference schemes for the computation of steady-state recirculating flows, *Comp. Meth. Appl. Mech. Eng.*, **23**, 293–312 (1980)
17 Huang, P. G., Launder, B. E. and Leschziner, M. A. Discretization of nonlinear convection processes: A broad-range comparison of four schemes, *Comp. Meth. Appl. Mech. Eng.*, **48**, 1–24 (1985)
18 Leonard, B. P. Simple high accuracy resolution program for convective modelling of discontinuities, *Int. J. Num. Meth. Fluids*, **8**, 1219–1318 (1988)
19 Leonard, B. P. and Mokhtari, S. Beyond first-order upwinding: The ULTRA-SHARP alternative for non-oscillatory steady-state simulation of convection, *Int. J. Num. Meth. Eng.*, **30**, 729–766 (1990)
20 Emmons, H. W. Evaluation committee report, in *Proc. 1980–81 AFOSR—HTTM—Stanford Conference on Complex Turbulent Flows*, Vol. II, pp. 979–986 (1981)
21 Demuren, A. O. Multigrid acceleration and turbulence models for computations of 3D turbulent jets in crossflow, *NASA TM 105306, ICOMP-91-20; CMOTT-91-09*, NASA Lewis Research Center, Cleveland, Ohio (1991)
22 Gosman, A. D. and Ideriah, F. J. K. TEACH-T: A general computer program for two-dimensional turbulent recirculating flows. Fluids Section, Department of Mechanical Engineering, Imperial College, London (1976)
23 *FLUENT*, Creare.X, Hanover, NH (1991).
24 Chung, B. T. F. Personal communication (1992).

25 Fletcher, C. A. J. *Computational Techniques for Fluid Dynamics*, Vols. I and II, Springer, New York (1988)
26 Ghia, U., Ghia, K. N. and Shin, C. T. High-Re solutions for incompressible flow using the Navier–Stokes equations and a multigrid method, *J. Comp. Phys.*, **48**, 387–411 (1982)
27 Hayase, T., Humphrey, J. A. C. and Grief, R. A consistently formulated QUICK scheme for fast and stable convergence using finite-volume iterative calculation procedures, *J. Comp. Phys.*, **98**, 108–118 (1992)
28 Godunov, S. K. Finite difference method for numerical computation of discontinuous solutions of the equation of fluid dynamics, *Matematik Sbornik*, **47**, 271–285 (1959)
29 Roe, P. L. and Baines, M. J. Algorithms for advection and shock problems, *Proc. 4th GAMM Conf. Num. Meth. Fluid Mech.* (Ed. H. Viviand), Vieweg, Germany, pp. 281–290 (1982)
30 Roe, P. L. *Annual Reviews of Fluid Mechanics*, Vol. 18 (Eds. M. Van Dyke, J. V. Wehausen and J. L. Lumley), Annual Reviews Inc., pp. 337–365 (1986)
31 Rachowicz, W., Oden, J. T. and Demkowicz, L. Toward a universal h–p adaptive finite-element strategy, Part 3. Design of h–p meshes, *Comp. Meth. Appl. Mech. Eng.*, **77**, 181–212 (1989)
32 Sweby, P. K. High resolution schemes using flux limiters for hyperbolic conservation laws, *SIAM J. Num. Anal.*, **21**, 995–1011 (1984)
33 Mokhtari, S. Development and analysis of steady high-resolution non-oscillatory convection schemes using higher-order upwinding, *PhD Dissertation*, University of Akron (1991)
34 Tzanos, C. P. Central difference-like approximation for the solution of the convection-diffusion equation, *Num. Heat Trans.* (*B*), **17**, 97–112 (1990)